The pre-submission synopsis (5000 words) is accepted and presentation may done accordingly. Recommended for final submission of the thesis.

PETROLOGY OF MAFIC-ULTRAMAFIC ROCKS AROUND BANGRIPOSI AND KULIANA, ORISSA, EASTERN INDIA: IMPLICATIONS FOR PALEOTECTONIC SETTING

Summary

By

TUSHAR MOULI CHAKRABORTI

Registration no. - R-14RS15110049

PRESIDENCY UNIVERSITY

KOLKATA

Supervisor

Dr. ARIJIT RAY

Co-supervisor

Dr. GAUTAM K. DEB

2017

PETROLOGY OF MAFIC-ULTRAMAFIC ROCKS AROUND BANGRIPOSI AND KULIANA, ORISSA, EASTERN INDIA: IMPLICATION FOR PALEOTECTONIC SETTING

STATEMENT OF PROBLEM & OBJECTIVES

The present work has been focused on a suite mafic-ultramafic rock, located in the eastern margin of Singhbhum Craton (SC) of eastern India (Fig. 1). The rock group consists of a modally layered gabbroic suite (dubbed as **"Kuliana Layered Gabbro" (KLG)**) (Fig. 2), and a Cr-spinel-bearing wehrlite suite (dubbed as **"Bangriposi Wehrlite" (BW)**) (Fig. 3), emplaced within the polydeformed metasedimnetary rocks of Singhbhum Group (SG), belonging to the North Singhbhum Mobile Belt (NSMB) assemblage (Saha, 1994). Although according to the most recent studies (Misra, 2006) these rocks have been identified as Mesoarchaean (3.09 Ga) units, there continue to exist a long-standing debate involving their petrogenetic and stratigraphic status. Thus, the present work has tried to answer some of the questions surrounding these rocks with the following objectives:

A. Geological mapping to understand the actual disposition of the rocks including relation among different units in space and relative time.

B. Field and petrographic studies of these mafic-ultramafic rocks will be carried out to characterize their different types and to correlate them with same rock groups in other parts of Indian Precambrian.

C. Recognition and characterization of different chemical types within the suite of the proposed area based on petrography, mineralogy and geochemistry, including isotope geochemistry.

D. Studies to understand nature of deformation of the country rocks adjacent to these rocks and primary/deformational fabric preserved in them. This will help to identify stratigraphic status of these mafic-ultramafic rocks.

F. Attempt will be made to develop a petrotectonic model using field and laboratory information hence a tectono-magmatic history of Singhbhum Craton in Proterozoic.

Overall, the fundamental objective of this research work has been to study and decipher the petrogenetic history of these individual suites of mafic and ultramafic rocks and then correlate them to assess the tectono-magmatic record of the study area, with implications for the tectono-magmatic history of Singhbhum Craton during the Archaean era.

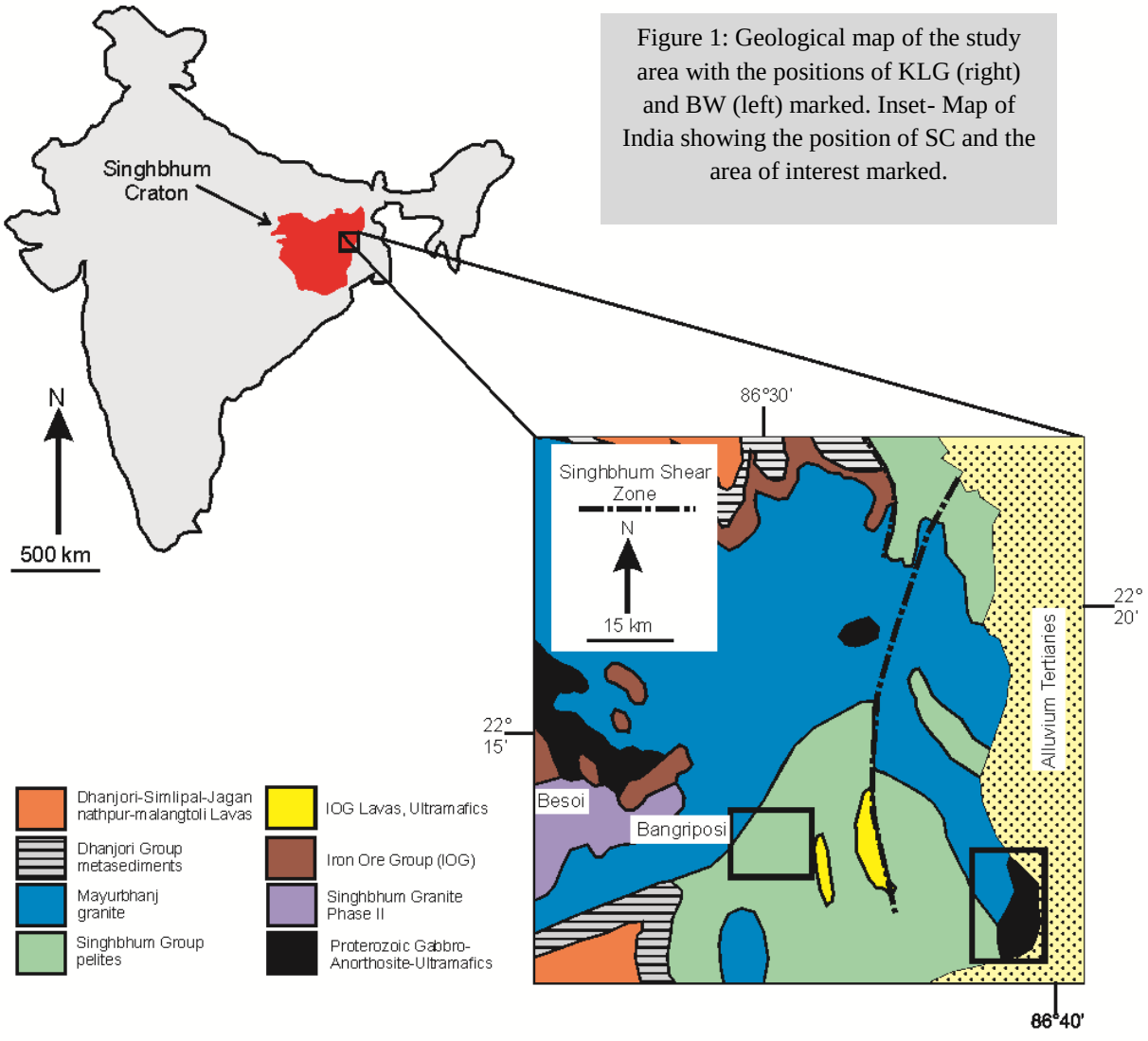

Figure 1: Geological map of the study area with the positions of KLG (right) and BW (left) marked. Inset- Map of India showing the position of SC and the area of interest marked.

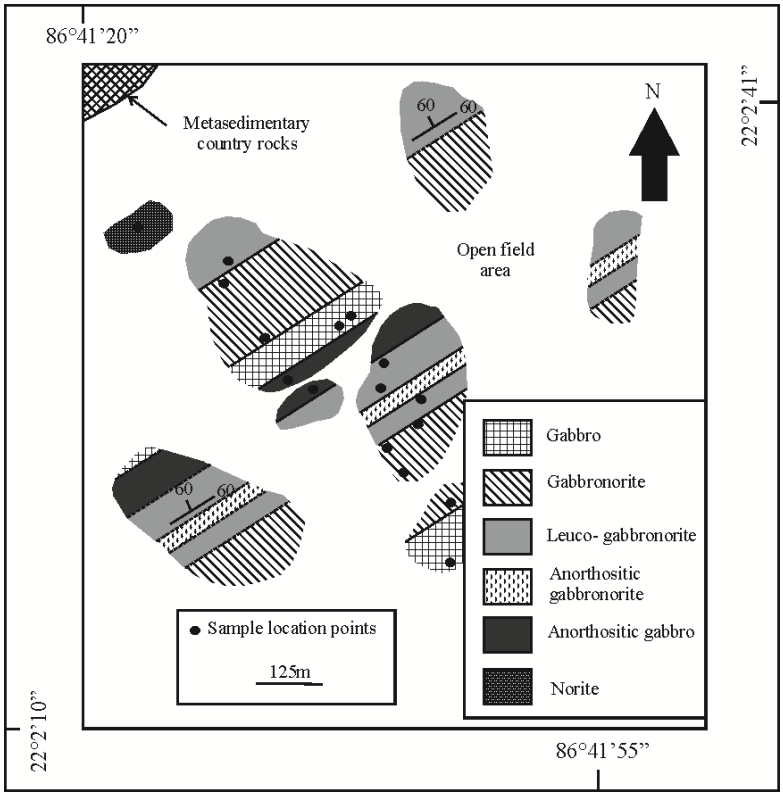

Figure 2: Lithological map of KLG with the modal layers drawn (Chakraborti et al., 2016)

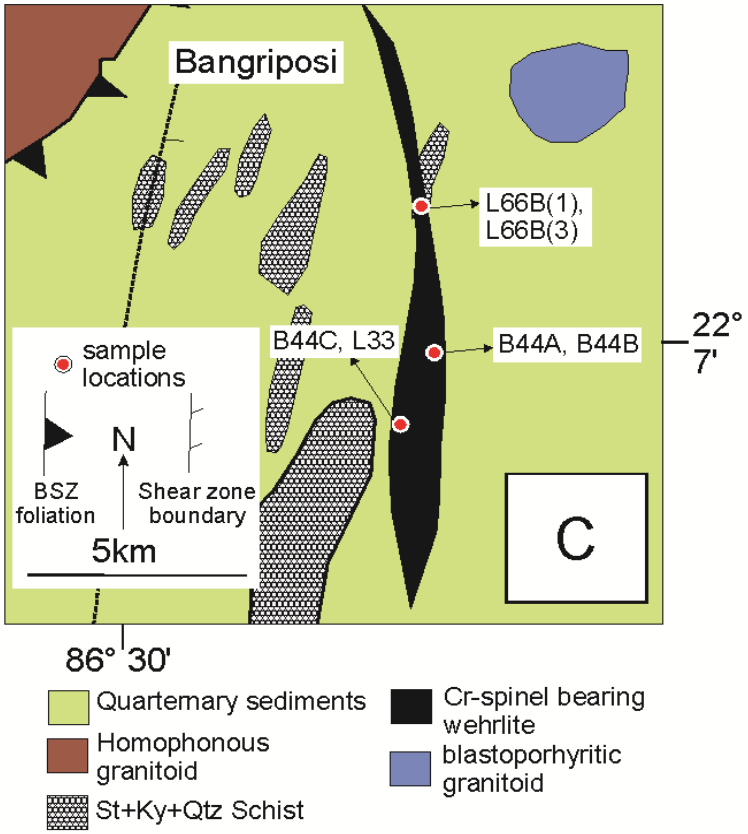

Figure 3: Geological map of BW suite and its surrounding area (modified after Prabhakar et al., 2014)

BRIEF SUMMARY OF RESULTS

1. Petrography

Petrographical study was performed on selected thin-sections of both rock groups in the facilities of Department of Geology, Presidency University, Kolkata. Preliminary analysis was done on Nikon advance high-resolution petrographic microscopes and subsequently, the Scanning Electron Microscopy (SEM) facility was used.

1.1. ***Kuliana Layered Gabbro:*** The Kuliana layered gabbro rocks are exposed in the field as massive, coarse-grained gabbroic rocks. However, on close observation mm- to cm-scale monomineralic laminations of both plagioclase and pyroxene were seen (Fig. 4a & 4b respectively). Compositional variations, manifesting as changes in the color index of the rocks (depending on the relative proportion of feldspar and pyroxene), were observed throughout the entire suite. Accordingly, samples were collected at places where this colour index variation was observable and the intervals between them were regularly measured. These sample points were plotted in the map and modal analysis was carried out on the representative thin-sections prepared from these samples. Depending on the observed modal

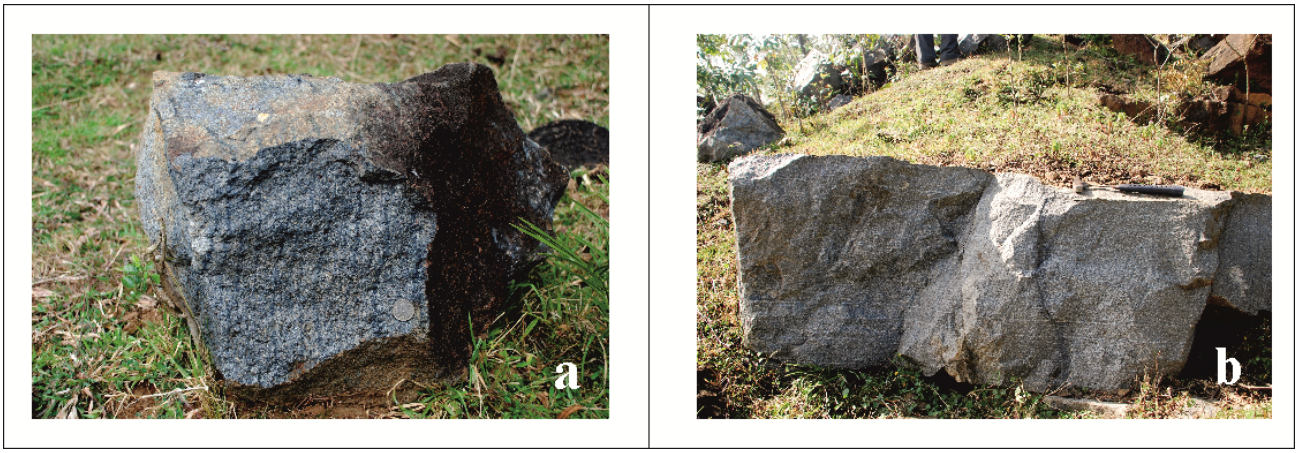

Figure 4: Field photographs of KLG- (a) laminations of pyroxene within gabbro; (b) laminations of plagioclase within anorthositic gabbro

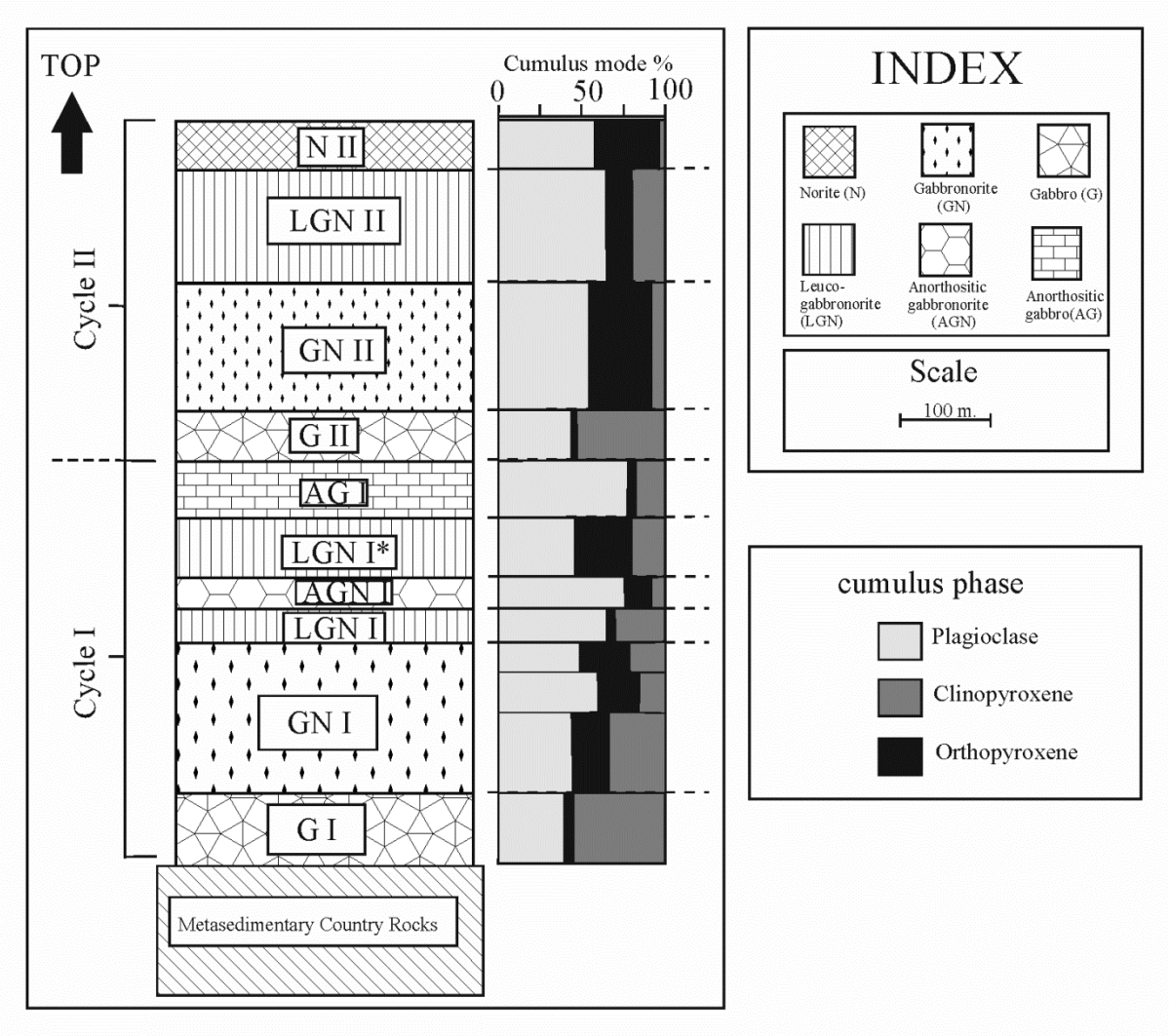

Figure 5: Litholog of the KLG with cumulus mode percent given for each modal layer (Chakraborti et al., 2017a).

variation, ten isomodal layers of variable thickness were identified and drawn on the map, following the measured strike of the monomineralic laminations. These ten isomodal layers were divided into two cycles based on rhythmic variations in modal proportions of feldspar (plagioclase)- Cycle I with six modal layers or litho units and Cycle II with four modal layers or litho units (Fig. 5) (Chakraborti et al., 2017). As mentioned earlier, the Kuliana suite occurs in the core region of a regional synform in the Singhbhum Group, and the NE-SW modal layers dip towards NW. There is no evidence of overturning in two limbs of the regional synform as evident from cross bedding and dip direction of bedding planes of

metasedimentary rocks. Thus the 60° NW dip of different modal layers of the layered gabbroic intrusive of Kuliana is likely to indicate younging direction. Moreover, Gradation in grain sizes in individual layers indicates younging in NW direction. Hence, cycle I, comprising of the six modal layers from the south-eastern part of the intrusion may be considered as the lower cycle or older cycle, and cycle II consisting of four modal layers, situated at the north-western part represents the upper or younger cycle.

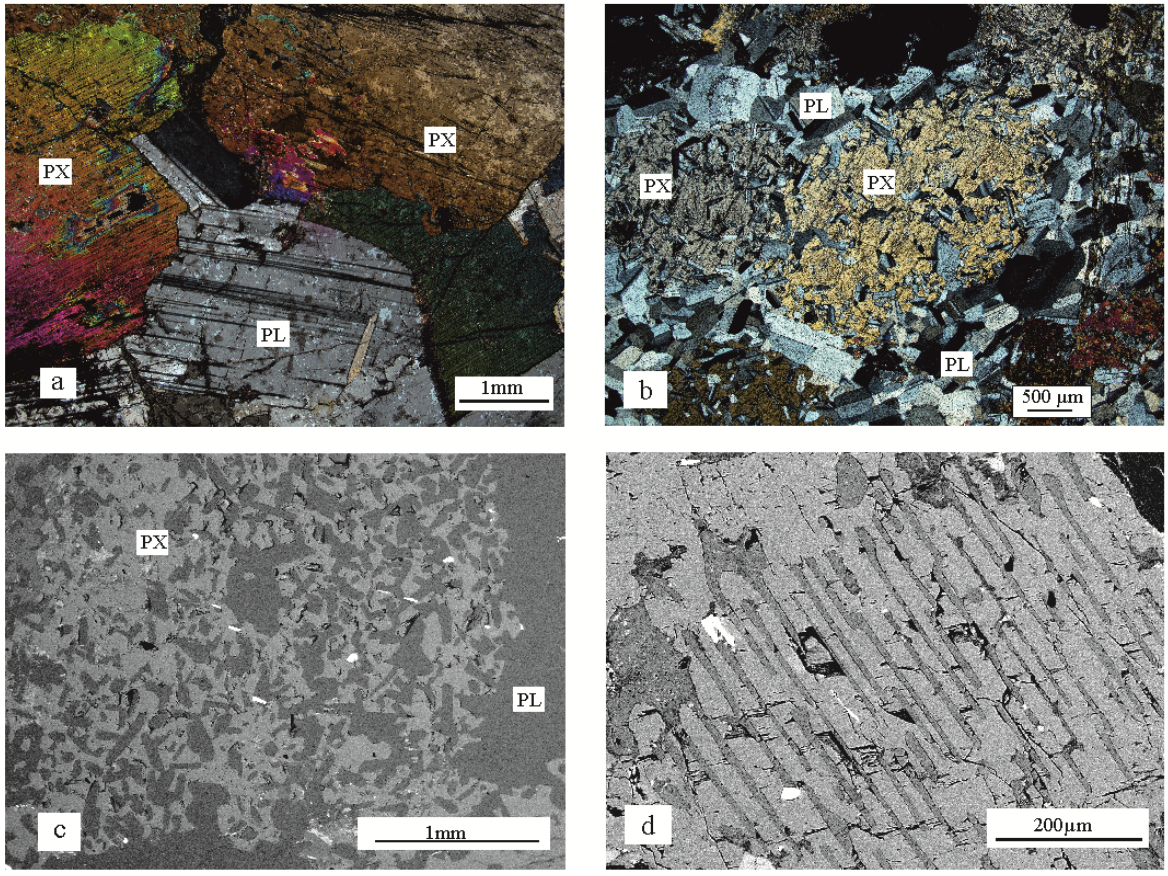

Figure 6: Photomicrographs of KLG- (a) cumulus texture under cross-polar; (b) poikilitic texture under cross-polars; (c) BSE image of an oikocrystic pyroxene; (d) BSE image of opx exsolution within cpx.

The rocks of the Kuliana gabbroic suite are essentially made up of plagioclase, orthopyroxene and clinopyroxene as cumulus phases, and intercumulus phases like illmenite, Cr-spinel, magnetite, and sulphide minerals (pyrite, chalcopyrite, arsenopyrite) are present as accessory. Ophitic and sub-ophitic textures are observed throughout the sequence. Both plagioclase and

pyroxene vary in size and shape within and across individual layer though out the whole cycle. In the bottom layers of either cycle, both plagioclase and pyroxene occur as coarse euhedral to subhedral grains in sharp contacts, defining cumulus texture (Fig. 6a). The upper layers of the Cycle I (LGN I, LGN I*and AG I) and N II layer of the Cycle II, on the other hand, are dominated by the poikilitic texture with marked bimodal size distribution of plagioclase (Fig. 6b). Such systematic variation in texture defines the textural layering of the suite. The GN I-LGN I contact is a thus a form contact and separates cumulate texture dominated lower part from poikilitic texture dominated upper portion in the Cycle I. The contact between the two cycles (AG I-G II contact) is a similar contact which separates the cumulate texture dominated basal layers of the Cycle II from the poikilitic texture dominated upper parts of the Cycle I. Finally, the LGN II-N II contact is another form contact demarcating the lower cumulus texture dominated part from upper poikilitic texture dominated N II layer. Poikilitic pyroxene grains in places host numerous tiny subhedral plagioclase laths as inclusions (Fig. 6c). No Imprint of deformation such as traces of secondary foliation, deformed twin lamellae in plagioclase is observed in the rocks of the Kuliana gabbro suite. Locally, coarse orthopyroxene grains in the bottom layers of both the cycles host exsolved clinopyroxene lamellae (Fig. 6d).

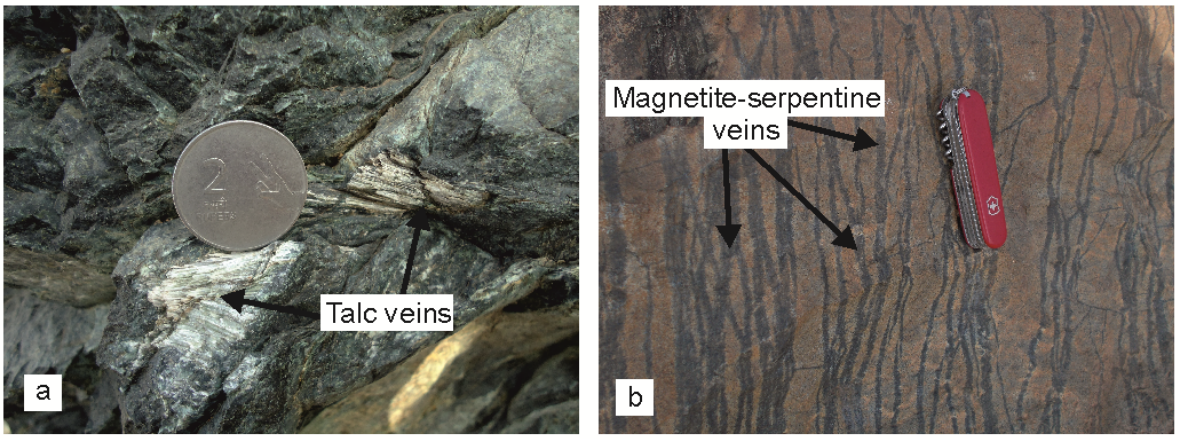

Figure 7: Field photographs of BW suite- (a) Talc veins; (b) magnetite-serpentine veins.

1.2. ***Bangriposi Wehrlite:*** The spinel-wehrlite body around Bangriposi is coarse grained and has a distinct dark greenish-black appearance, which is largely due to the low grade metamorphic alteration suffered by these rocks. Talc veins (Fig. 7a) characterize the more highly altered parts in the field. Networks of magnetite-serpentine veins within the wehrlite body are also seen in some places (Fig. 7b). The modal compositions of the rocks are Cr-spinel bearing wehrlite, and the principle mineral constituents are serpentine, clinopyroxene, Cr-spinel, vermiculite, magnetite, with minor amounts of apatite and ilmenite, and accessory phases such as talc, brucite and tremolite. Vermiculite is a platy mineral much similar to mica with a hydrated silicate composition, and they mostly form due to replacement of K by Mg during hydrothermal alteration processes. Under petrographic microscope, the overall effect of Serpentinization is conspicuous. Almost all larger olivine grains have been largely replaced by serpentine keeping the grain boundary intact (pseudo morphs), whereas, the smaller olivines have lost their shape and the original aggregate of olivine grains has been transformed to patches of cross-cutting serpentine veins, exhibiting mesh-texture and hosting numerous magnetite grains (Fig. 8a). Magnetite is also seen in the groundmass forming vein like networks. Only the olivine grains occurring as inclusions within pyroxene grains are less altered and give relict olivine compositions. Clinopyroxene grains are relatively less affected by the alteration process. Some have a brownish appearance under crossed polars and host fibrous aggregate of tremolite and magnetite veins along cleavage plains and fractures. Relict or partially relict portions of clinopyroxene grains can be observed having proto-granular texture. Kinking of cleavages across multiple parallel shear surfaces is visible in some relict clinopyroxene grains (Fig. 7b), which serves as evidence for tectonic deformation. Secondary clinopyroxene grains occurring as rims around olivine are often seen (Fig. 7c). Vermiculite occurs exclusively as interstitial patches around olivine grains rimmed by clinopyroxene, and not as primary, discrete grains (Fig. 7c). Primary grains of orthopyroxene are almost absent,

but orthopyroxene is sometimes found as secondary reaction rims around some olivine grains (Fig. 7d). Cr-spinel grains have retained their magmatic euhedral/subhedral shapes, although at places they exhibit evidence of sub-grain formation due to metamorphic re-crystallization (Fig. 7e). Magnetite mantles around Cr-Spinel grains are also seen. Apatite occurs both as interstitial lamellae and adjacent to zones of magnetite crystallization (Fig. 7f).

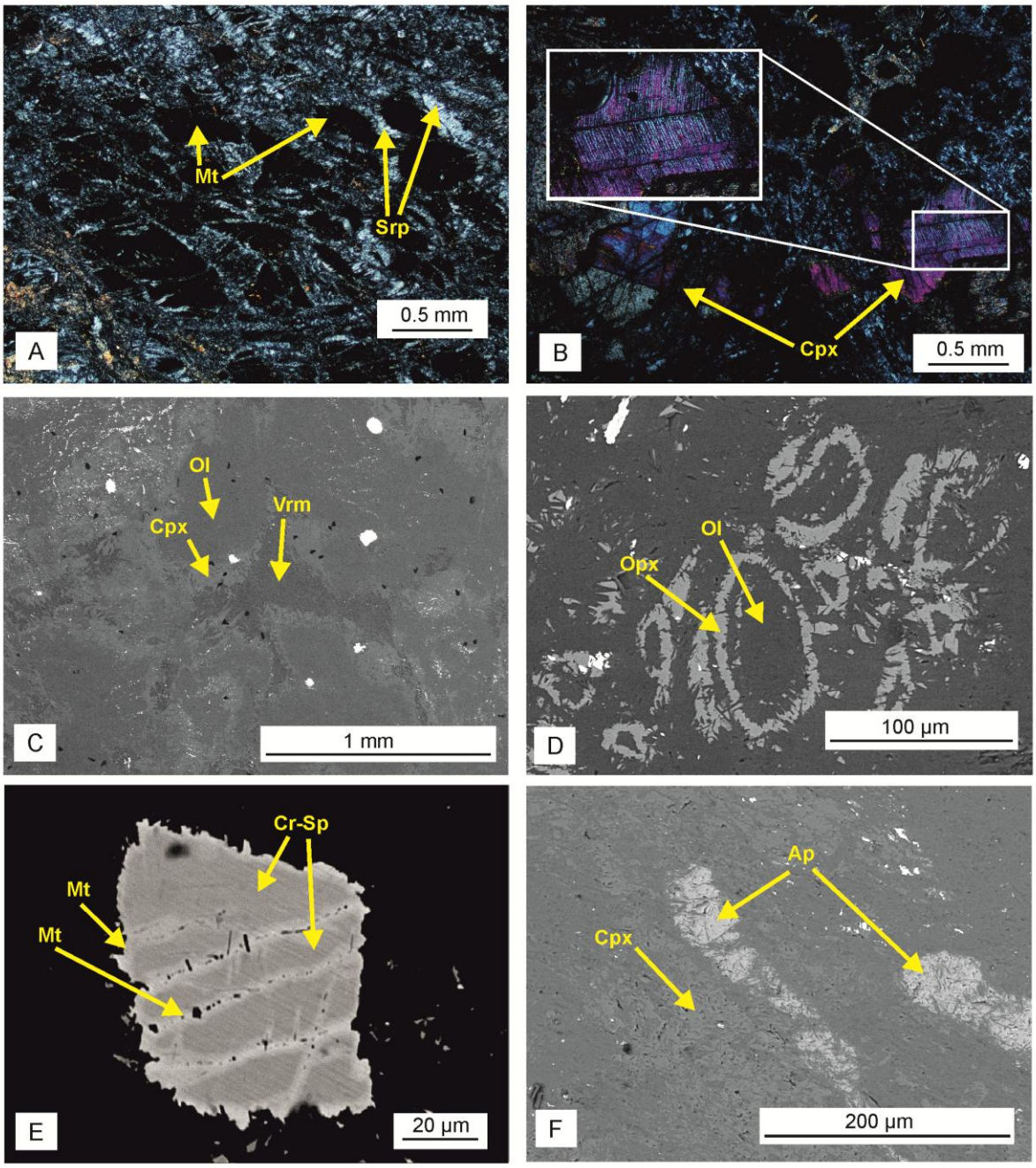

Figure 8: Photomicrographs of BW suite- (a) mesh texture; (b) kink bands in px cleavage surfaces; (c) development of phlogopite as reaction texture; (d) opx rim formation around serpentinised olivine grain; (e) Sub-grain formation and magnetite mantles in Cr-spinel grain; (f) secondary apatite formation.

4. Mineralogy

4.1. Kuliana Layered Gabbro: Mineral chemistry was performed on selected thin-sections in the Department of Geology and Geophysics, IIT Kharagpur, using the CAMECA SX100 Electron Probe Micro Analyzer (EPMA). The operating conditions were 15kv of voltage and 20nA of current.

4.1.1. Plagioclase- Two generation of plagioclase grains (An_{55}-An_{65} and An_{75}-An_{85}) can be identified form layers of the KLG. G I and GN II layers have less calcic (An_{57}- An_{66}) plagioclase in the groundmass than plagioclase grains occurring as inclusions (An_{78}- An_{85}).

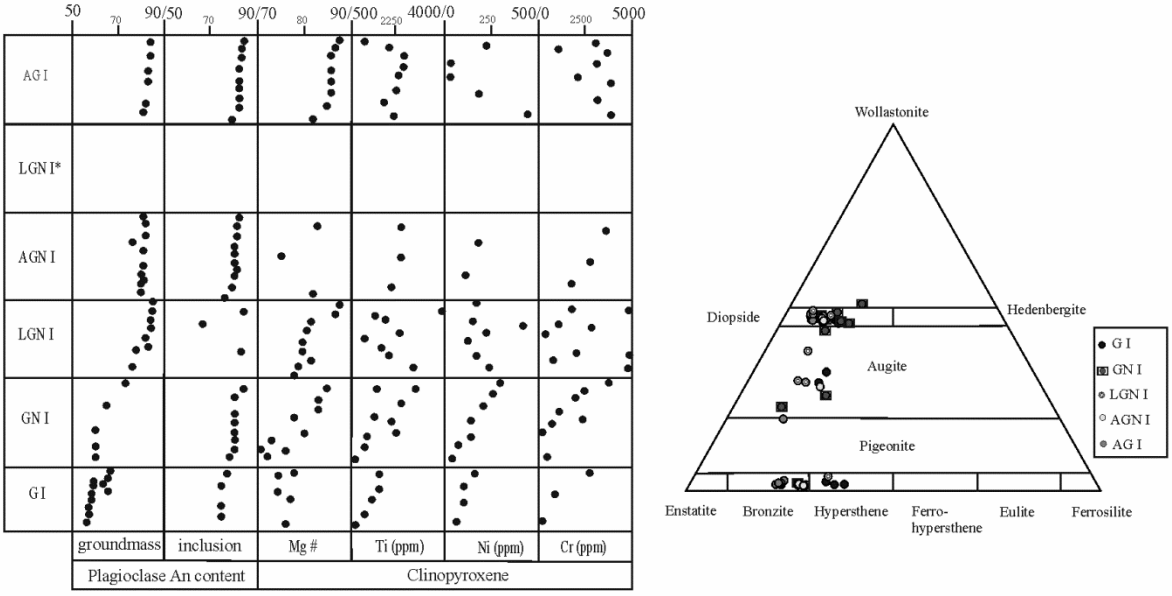

Figure 9: (a) Layer wise variation of selected mineralogical parameters of Cycle I rocks from KLG; (b) End-member compositional plot of pyroxene grains from the KLG.

The groundmass plagioclase grains become abruptly more calcic (An_{76}- An_{85}) in the upper parts of GN I and in the LGN I layers. From this point onward in cycle I, both groundmass plagioclase and plagioclase grains exhibit almost identical compositions (An_{76}- An_{85}) up to the topmost layer of Cycle I (Fig. 9a). Some plagioclase grains in the groundmass of LGN I and GN I display high magnitude reverse zoning. The difference in composition between the plagioclase grains from groundmass and those occurring as inclusions in G I and GN I may

possibly be a result of polybaric crystallization process. In that case, the more calcic plagioclase inclusions formed at an early stage and later were trapped in the pyroxene grains. The abrupt change in composition of groundmass plagioclase grains from the upper parts of GN I to LGN I and further upwards, indicate a possible event of magma chamber replenishment. Reverse zoning of high magnitude observed in some plagioclase grains in the groundmass from GN I and LGN I, lends evidence in support of the probable magma influx event.

4.1.2. Clinopyroxene- Two compositional varieties exist in the clinopyroxene grains from the KLG suite - diopside, and augite (Fig. 9b). Grains from AGN I and AG I display significantly less scatter in the compositional plots relative to the grains from G I, GN I and LGN I. Mg# values increase from G I and GN I (range: 69-82; avg: 76) to LGN I (range: 79-88; avg: 82) and remain more or less similar in AGN I (Fig. 9a). Cr concentrations in the clinopyroxene reflect similar variation patterns of sharp increase from GN I to LGN I, followed by a minor drop in concentration in AGN I and subsequent increase in AG I. While Ni concentrations show a steady increase up to LGN I and then declines and remains stable up to AG I. Ti concentrations on the other hand display a marked increase up to AGN I, followed by a minor decrease in AG I. The imprint of a possible magma influx event can also be observed from the compositional variation of the clinopyroxene grains (Fig. 9a), manifesting as a sharp increase in average Mg#, Cr and Ni content across the GN I-LGN I interface. Thus, based on combined mineralogical changes observed across this interface, the GN I-LGN I contact can be said to define cryptic layering.

4.1.3. Orthopyroxene- Orthopyroxene grains plot in the bronzite and hypersthene field (Fig. 9b). Although a general trend of increasing En content and Cr abundance of orthopyroxene is apparent (Fig. 9a), emphasis on the layer wise variations of these parameters is not given due to lack of adequate analytical data.

4.2. Bangriposi Wehrlite: The EPMA facility of Indian School of Mines (ISM), Dhanbad comprising of CAMECA SX5 instrument, was used for analysis. The operating conditions were 15kv of voltage and 15nA of current. Along with EPMA analysis, X-Ray Diffraction (XRD) analysis was also performed on the ultramafic rocks for identification of the constituent minerals (Fig. 10a). The XRD facility at Central Glass & Ceramic Research Institute (CGCRI) was used.

4.2.1. Serpentine- Most of the serpentine grains have Fo_{82}- Fo_{93}, possibly reflecting Mg enrichment with progressive hydrothermal alteration. Their total major oxide values range from 86% - 89% because of high volatile contents commonly seen in serpentine group of minerals. Mg# (100Mg/Mg+Fe) ranges from 80-86 with some as low as 72-73. Ni contents are high with an average of 1645 ppm and some even as high as 2400 ppm. They also have relatively higher Al_2O_3 contents of 1.5%- 3.5%. There is no significant change in composition between two modes of occurrence of the serpentinized olivine grains- as inclusions and as grains in the groundmass. XRD analysis revealed that the predominant species of serpentine present are antigorite and lizardite, with minor occurrences of chrysotile.

4.2.2. Clinopyroxene- Clinopyroxene grains have major oxide totals of 96%- 100%, which suggests their variable volatile content is due to the presence of tremolites along grain fractures and margins. The clinopyroxene grains suffered this amphibolitization process during serpentinization. The clinopyroxene grain population consists of two species (Fig. 10b) - Augite (more abundant) with compositional ranges of Wo_{24-28} En_{62-68} Fs_{4-11}, and Near Diopsidic with composition Wo_{41-44} En_{47-51} Fs_{7-8}. The Mg# of augite grains are 78- 91 and relatively low (75- 80) for Diopside grains. They are low in Na_2O, Al_2O_3, TiO_2, and Cr_2O_3.

XRD analysis revealed the presence of tremolite- actinolite grains, which formed during low-grade metamorphism at clinopyroxene grain margins.

4.2.3. Orthopyroxene- Orthopyroxene grains are mainly found as reaction rims around some olivine grains, as mentioned in the petrography section. These have bronzite

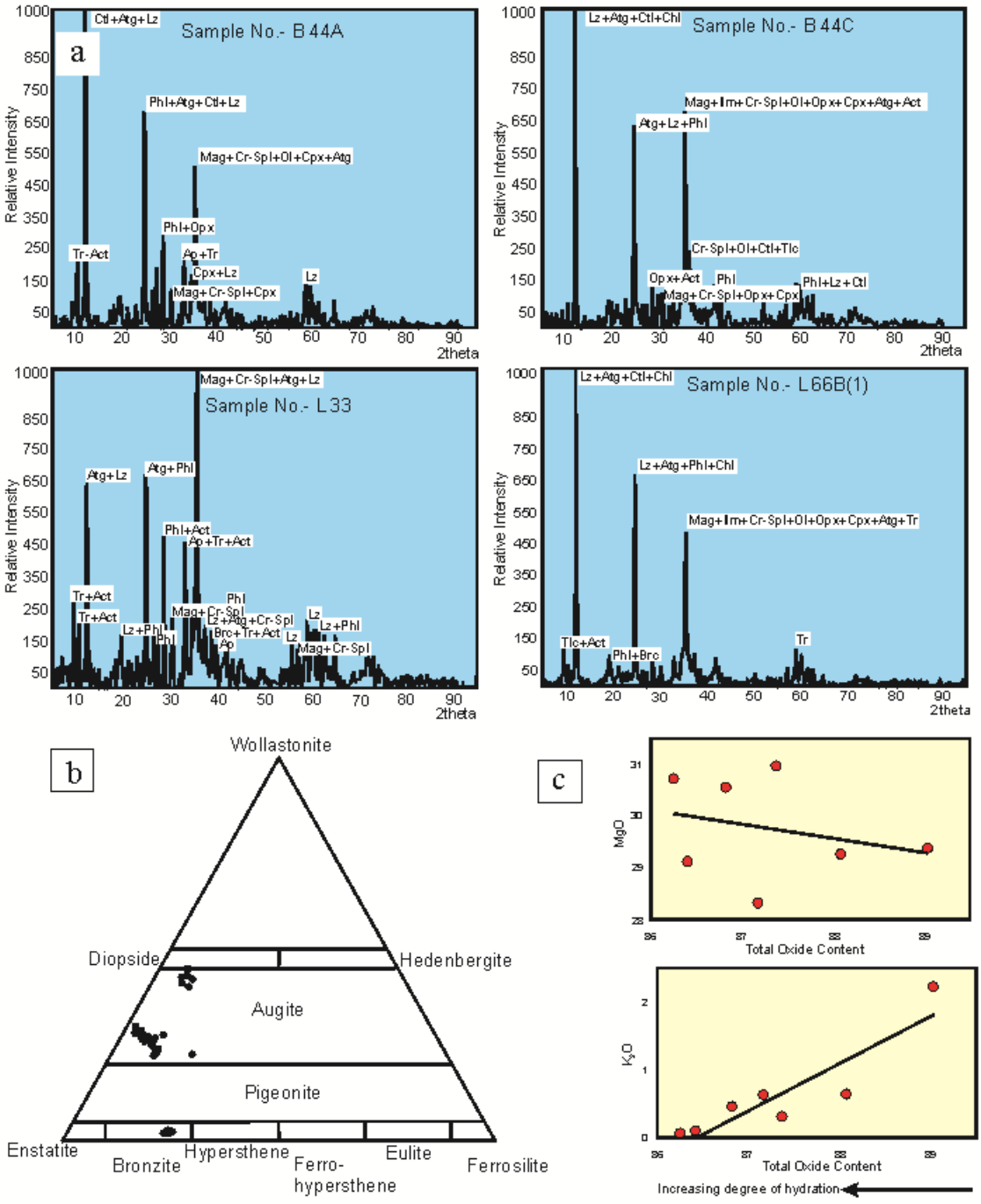

Figure 10: (a) Relative intensity vs 2Θ plots of BW rocks; (b) End-member compositional diagram of pyroxene grains from BW; (c) MgO/K2O vs Total oxide content plot of rocks from BW suite.

compositions (Fig. 10b) and their mg# are between 62- 63 with high Ni contents of >3000 ppm. Orthopyroxene is also found as rare relict grains in association with secondary clinopyroxene and olivine.

4.2.4. Cr-spinel- Cr-spinels have high Cr# (100Cr/Cr+Al) with with ranges from 77- 92 and very low MgO contents, which are reflected in their Mg# range of 4-20. Values of TiO_2 are 1%- 3.3 % and MnO values are 1.3%- 1.9%. Most euhedral spinel grains exhibit compositional zoning, where the core of the grains is Cr-Al rich and the margin is Cr-Al poor (Fig. 8e). This type of zoning is also observed in Cr-spinel grains which exhibit sub-grain formation, in which case, individual sub-grains display this zoning pattern.

4.2.5. Vermiculite- The presence of vermiculite was unclear from the EPMA analysis, as these grains only revealed a hydrated ferro magnesian silicate composition rich in Al_2O_3 with little amount of K_2O. This could either have been a low K_2O phlogopite or hydrated pyrope garnet. However, the atomic structure of mica was found in the XRD results, which confirmed the existence of vermiculite. The vermiculite grains form because of hydrothermal alteration of phlogopite grains. The alteration process involves replacement of the interlayer K with Mg. The K_2O values decrease with increasing degree of hydration (corresponding to decreasing total of wt% major oxide contents) and increasing the content of MgO (Fig. 10c). The K_2O values (0.04- 2.2%) of these grains are comparable with K_2O contents of vermiculite occurrences from different parts of the world. Their Mg# has a restricted range of 74- 82, whereas K# (100K/K+Na) has more variable range of 40- 95.

4.2.6. Accessory- Apatite, Ilmenite and magnetite occur as the main types of accessory mineral species. Minor amounts of tremolites are seen along clinopyroxene grain margins. XRD analysis also revealed the presence of talc and brucite.

5. Geochemistry

Chemical data for the samples were determined at the Geochemical Laboratory of the Wadia Institute of Himalayan Geology (WIHG), Dehradun. Major elements were determined using the X-ray Fluorescence (XRF) (SIEMENS SRS 3000) facility. Analysis of major elements by XRF has over 95% accuracy. Trace elements, including REE were determined by Inductively Coupled Plasma- Mass Spectrometry (ICP-MS) (PerkinElmer SCIEX ELANDRCe) and the sample dissolution procedure of Khanna et al. (2009) was followed.

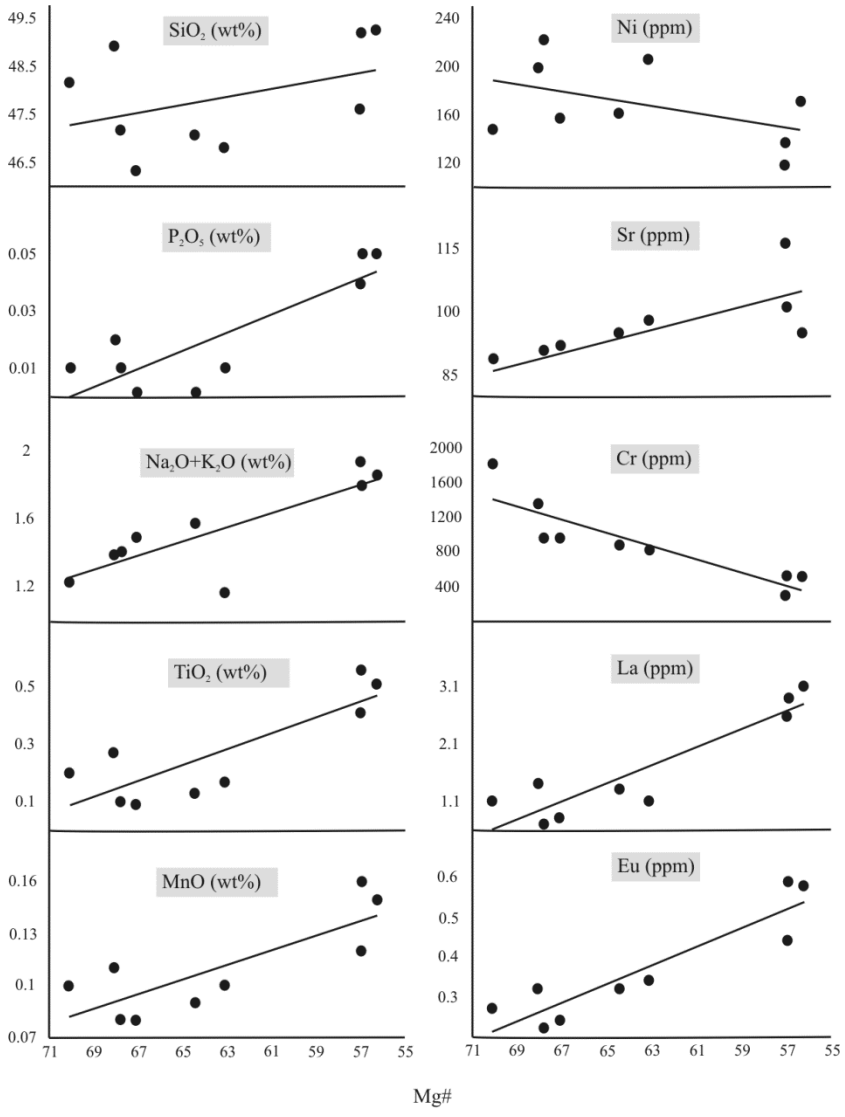

Figure 11: Bi-axial variation diagram of selected major and trace elements against Mg# from KLG suite.

5.1. Kuliana Layered Gabbro: SiO_2 of the rocks varies from 46% to 49%, (Na_2O+K_2O) content varies from 1.2% to 1.9%, and Mg# (100Mg/ Mg+Fe) ranges from 56-70. Plots of some major element oxide like SiO_2, Na_2O+K_2O, P_2O_5, MnO, TiO_2 and trace element like Ni, Sr, Cr, La, Eu concentrations against Mg# (Fig. 11) display a increasing trends with decreasing Mg#. The opposite trends for Cr and Ni abundances are observed. Fractionation of plagioclase, clinopyroxene and orthopyroxene accounts for the dominant increasing trend observed in the biaxial variation diagrams. Primitive mantle normalized (Normalizing values are after McDonough and Sun 1995) spider diagram (Fig. 12a) depicts an overall

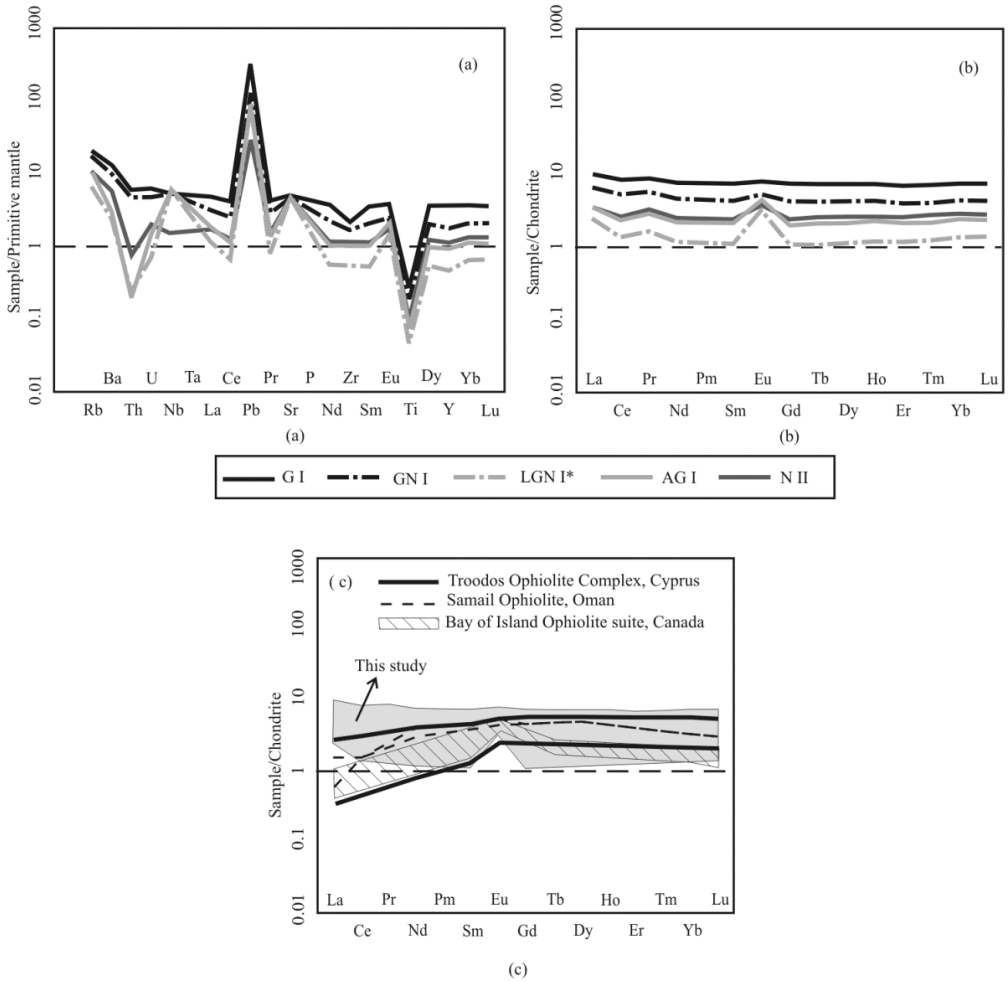

Figure 12: KLG Trace and REE plots- (a) Primitive mantle normalized spider plot; (b) Chondrite-normalized REE abundance diagram; (c) REE comparison with ophiolitic gabbros (Chakraborti *et al*., 2016).

prominent Pb peak and marked Ti depletion. Slight LILE (Rb, Ba, Th, U) enrichment is shown by G I and GN I, along with a mild Zr trough. Patterns for LGN I*, AG I and N II

follow almost similar characteristics, with the exception of a trough at Th. The trace element profile of the Kuliana layered gabbro- rocks reveal their relatively depleted geochemical nature and both in spider plots and REE abundance plots the values fall between 1 to 10 times the normalizing values. Chondrite normalized (Normalizing values are after Boynton, 1984) rare earth element profiles (Fig. 12b) present a reasonably unfractionated pattern of the layered cumulate rocks. Positive Eu anomaly is observed and becomes progressively more conspicuous with the increase in modal plagioclase content.REE patterns of the Kuliana layered suite are similar to REE patterns of cumulate gabbro sections of ophiolites, as seen in the comparison diagram (Fig. 12c). It is evident from the spider and REE plots that the source region of the Kuliana gabbro-anorthosite rocks was depleted in nature. Although selective element (LILE and LREE) enrichment is observed, the degree of enrichment is relatively low.

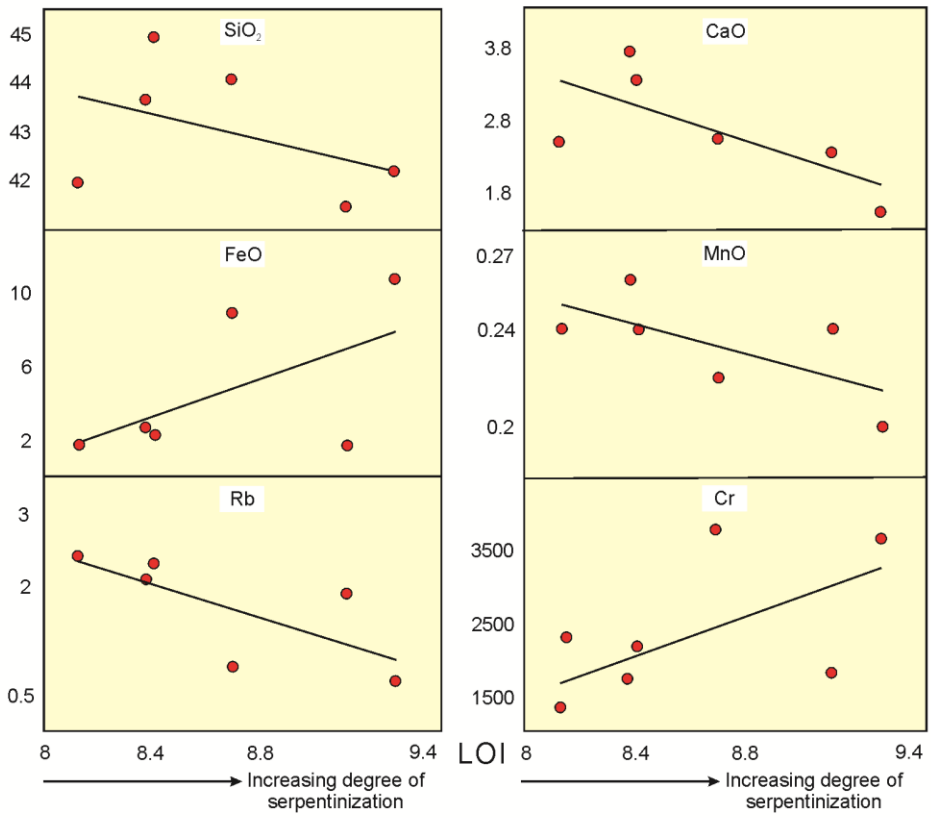

Figure 13: Bi-axial variation diagram of selected geochemical parameters plotted against LOI.

5.2. Bangriposi Wehrlite: Extensive serpentinization affecting these ultramafic rocks is directly reflected in their high LOI content of 8- 9.3%. The SiO_2 content of wehrlite ranges from 41- 44% and consequently they have very low Differentiation Index (D.I.) values of 1.02- 1.3, suggesting their primitive nature. The Mg# of these rocks is relatively low (72- 77) when compared to other ultramafic rocks, but that can be attributed to elevated total FeO contents (12- 15%) due to magnetite crystallization during serpentinization. The effects of pervasive serpentinization are also evident from depleted alkali contents (Na_2O+K_2O) of 0.13- 0.17%. Low content of CaO (1.5- 3.3%) possibly reflect the dominance of olivine over clinopyroxene. The Cr (1350- 3700 ppm) and Ni (900- 2200 ppm) contents are relatively high, due to the high modal abundance of Cr-Spinel and serpentinized olivine. Although

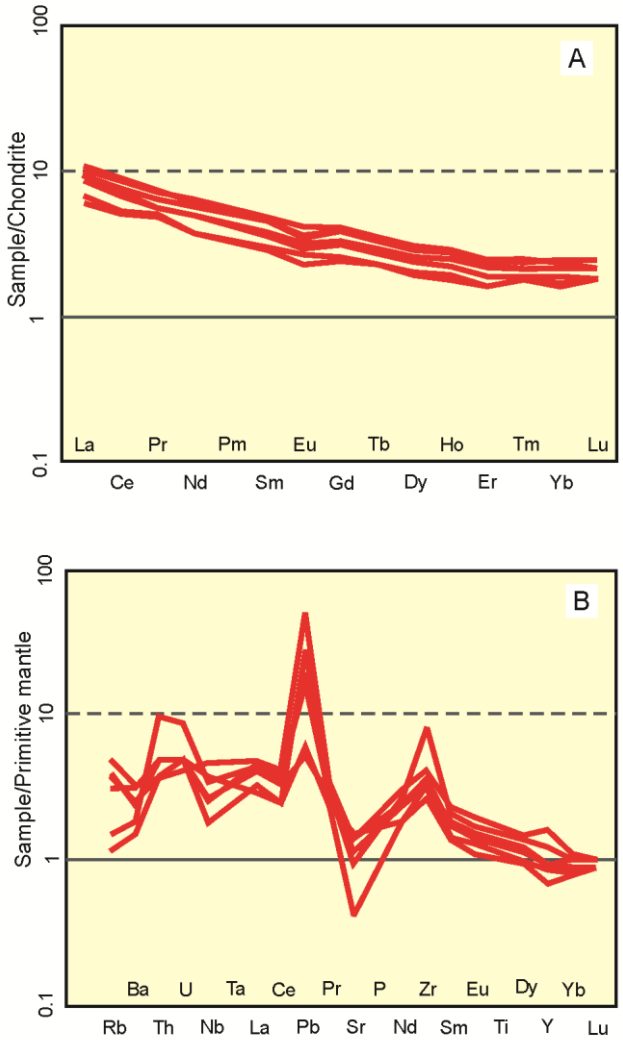

Figure 14: Trace and REE plots of BW rocks- (a) chondrite-normalized REE abundance diagram; (b) primitive mantle normalized spider diagram.

limited data on the variation diagrams makes it a bit difficult to comprehend, relatively negative correlations between LOI and CaO, SiO_2, MnO and Rb (Fig. 13) show the mobile nature of these oxides and elements during the serpentinization process. On the other hand, more conspicuous increasing trends of FeO and Cr record crystallization of secondary magnetite, chromite, during progressive serpentinization. Significant LREE enrichment is observed (Fig. 14a; normalizing values after Boynton, 1984) in these rocks (of the order of 10 times chondrite values) and $(La/Yb)_N$ ratios range from 3.6- 4.9. HREEs show mild depletion, but there is still a slight relative enrichment over chondritic levels. Subsequently, some LILEs (Ba, Th, and U) also have enrichment peaks in primitive mantle normalized plots (Fig. 14b; normalizing values after McDonough and Sun 1995), with accompanying enrichment in Pb and Zr. Distinct depletion troughs can be seen at Sr and Nb and some of the heavier elements (Dy, Y, Yb and Lu) show systematic depletion patterns.

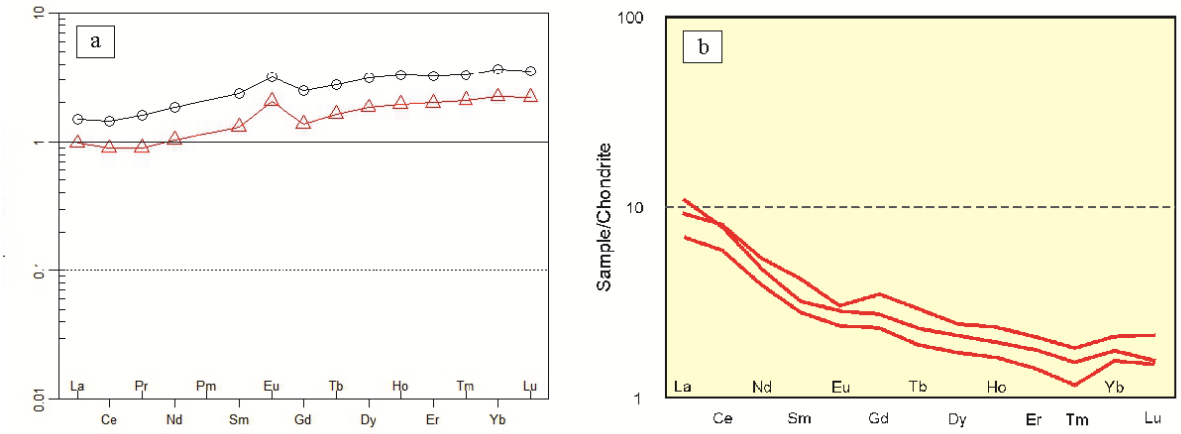

Figure 15: Chondrite-normalized REE abundance diagram of px separates- (a) from KLG rocks; (b) from BW rocks

5.3. Geochemistry of mineral separates: Plagioclase and pyroxene separates from the KLG suite were analyzed for trace and REEs in the Indian Institute of Science (IISc), Bangalore using Inductively Coupled Plasma-Mass Analyzer (ICP-MS) facility. On plotting in chondrite normalized REE plots (Fig. 15a), the plagioclase show a strong Eu peak, with

HREE depletion, whereas, the pyroxene exhibit relatively flat trends with slight HREE enrichment. Three pyroxene mineral separates from the Bangriposi wehrlite rock gropup were also analyzed for REE in the ICP-MS facility of Wadia Institute of Himalayan Geology (WIHG). These when plotted in chondrite normalized REE diagrams (Fig. 15b), show LREE enriched patterns.

6. Isotopic Analysis

Sr-Nd isotopic analysis was performed on whole rock samples from both KLG and BW suite. The analysis was carried out in the ICP-MS & Thermal Ionisation Mass Spectrometry (TIMS) laboratory in the Centre for Earth Sciences (CEaS), Indian Institute of Science (IISc), Bangalore, India. The TIMS instrument used was a Thermo Triton Plus, and sample dissolution and analytical procedure of Banerjee et al. (2016) was followed. Measured $^{143}/^{144}$Nd and $^{87}/^{86}$Sr ratios were normalized to $^{146/144}$Nd = 0.7219 and $^{86}/^{88}$Sr = 0.1194 respectively, to correct for instrumental mass fractionation. JNdi-1 Nd and SRM-987 Sr isotopic standard was analyzed during the course of the Sr-Nd analysis.

The KLG rocks exhibit slightly positive to negative ε_{Nd} (3.09 Ga) values (1.5 to -4.4), moderately low initial $^{143/144}$Nd (0.5084- 0.508697), and variable initial $^{87}/^{86}$Sr (0.7016- 0.7085). BW rocks on the other hand display high degrees of variability both in $^{143}/^{144}$Nd and $^{87}/^{86}$Sr values (0.507801- 0.508368 and 0.7054- 0.7228 respectively) and hence extremely low ε_{Nd} (3.09 Ga) values of -5.0 to -16.2. The complex metsomatic history of the BW rocks (Chakraborti et al., 2017b) is largely responsible for their extreme Sr-Nd isotopic character. However KLG rocks show little evidence of deformation or metasomatism and hence, their Nd isotopic character can be said to reflect the source region of these rocks. Calculated ^{147}Sm/ ^{144}Nd of the source region of the KLG rocks (0.1869; 5% less than

CHUR) also show enriched nature and the Fractionation Factor (α) of 1.05 corresponds with melting from a garnet bearing source region. Depleted mantle model age (T_{DM}) calculations of the mafic-ultramafic rocks yield a span of 3.6- 5.6 Ga.

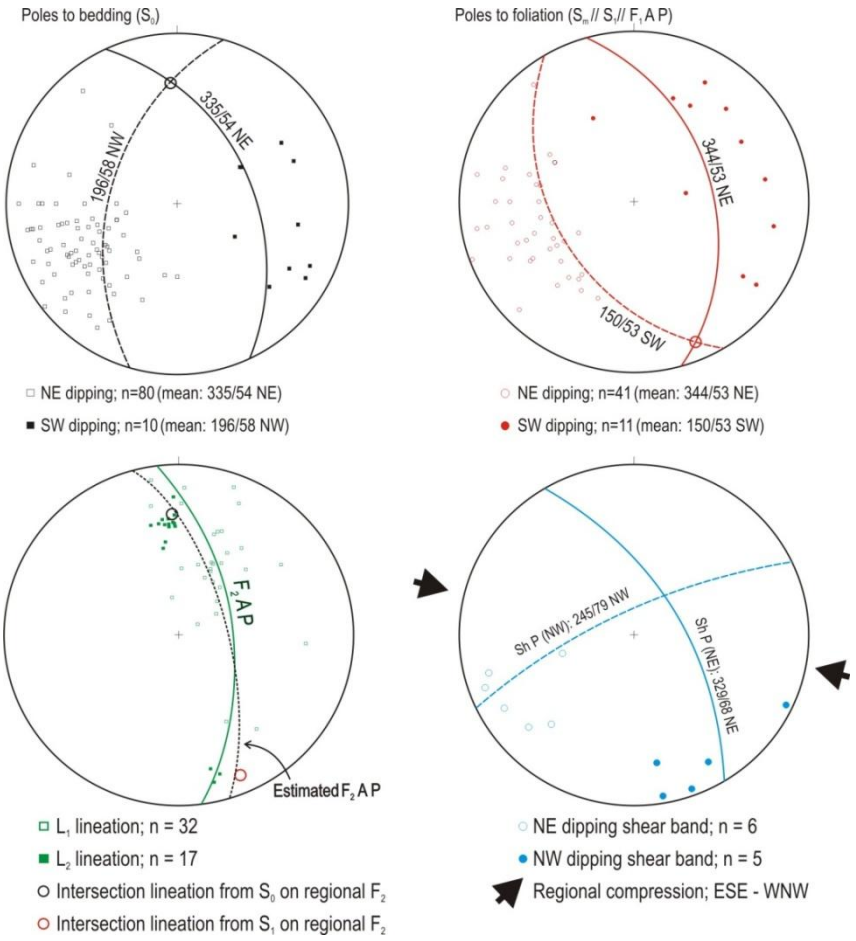
Poles to bedding (S0)
335/54 NE
196/58 NW
NE dipping; n=80 (mean: 335/54 NE)
SW dipping; n=10 (mean: 196/58 NW)
Poles to foliation (Sm // S1 // F1 A P)
344/53 NE
150/53 SW
NE dipping; n=41 (mean: 344/53 NE)
SW dipping; n=11 (mean: 150/53 SW)
F2 A P
Estimated F2 A P
L1 lineation; n = 32
L2 lineation; n = 17
Intersection lineation from S0 on regional F2
Intersection lineation from S1 on regional F2
Sh P (NW): 245/79 NW
Sh P (NE): 329/68 NE
NE dipping shear band; n = 6
NW dipping shear band; n = 5
Regional compression; ESE - WNW

Figure 16: Equal area projection diagrams of the metasedimentary country rocks around Kuliana.

7. STRUCTURE

7.1. Equal area projection diagrams: To understand the orientation pattern of different structural elements of the metasedimentary country rocks, poles to planner and linear structures were plotted in equal area projection diagrams. A total number of 90 bedding planes were measured especially from quartzites and 52 foliation measurements were done

from adjoining mica-schist rocks. Poles to bedding (S0) form two girdles representing mean bedding on two limbs of regional fold as 335/54 NE and 196/58 NW (Fig. 16). Similarly poles to mineral foliation (S_1), mylonitic foliation (S_m) and F_1 fold axial planes form two girdles representing mean F_1 foliations, 344/53 NE and 150/53 SW, which are folded by F_2 fold about a SSE plunging axis (Fig. 16). Remarkably many plots of bedding poles coincide with that of the mineral foliation, indicating near isoclinal geometry of F_1 folds on bedding which is also evident in the field. Plots of the mineral lineation (L_1) are spread over a girdle, 353/65 E, and thus representing F_2 axial plane. L_2 lineation includes puckers and F_2 axis. Plots of L_2 form two crude clusters, one plunging NNW and the other towards SSE. These two L_2 clusters are very close to the deduced F_2 axial plane that passes through L_1 lineations too (Fig. 16). Thus, the orientation pattern of these elements definitely indicates co-axial refolding of F_1 by F_2. Poles to shear bands form two crude clusters, and the mean shear bands are 329/68 NE and 065/79 NW. The regional compression that caused progressive deformation of these rocks was thus ESE-WNW (Fig. 16).

7.2. Strain analysis: The Bangriposi quartzite that outlines the regional map pattern hosts a few lenses of conglomerate, either polymictic with 1 to 5 cm pebbles of quartz, quartzite and chert, or oligomictic with 3 or 4 to maximum 20 cm pebbles of quartz. The quartz pebble conglomerate is essentially matrix supported conglomerate with the pebbles set in a gritty to coarse quartzite, and occurs as a 100 x 50 m lense near Kathasirsi, NW of Kuliana. Besides loose pebbles two orthogonal sections, both perpendicular to the regional foliation (XY) and the downdip lineation (i.e., YZ section) and sections nearly perpendicular to foliation and parallel to lineation (i.e., XZ section) are well preserved in this outcrop. The analysis has been carried out based on direct measurement of loose pebbles and from the photographic

images of the plan and oblique sections of the outcrops of the quartz pebble conglomerate. The findings of the study area around Bangriposi can be summarised as below-

1> The metasedimentary rock assemblage is characterised by repetition of sand (quartzose rock) – mud (argillaceous rock) pile on different scale.

2> The metasediments dominated lithologic assemblage is comparable to the Chaibasa Formation, the lower unit of the Singbhum Group.

3> Two methods, (i) direct pebble measurement and (ii) R_ϕ-ϕ after Ramsay (1967) and Ramsay and Huber (1983) have been employed separately to estimate how much strain the quartz pebbles of the Bangriposi conglomerate at Kathasirsi, near Kuliana enjoyed. The results of axial ratio (X Y: Z) and of *k*-value determined by these three methods are given in Table.

Method	Axial ratio (X:Y:Z)	*K*
Direct measurement	1.89 : 1 : 0.37	0.502
R_f-ϕ method	1.02 : 1: 0.21	0.007

Now the results indicate that the pebbles of the Bangriposi conglomerate and, in turn, all the rocks of the area deformed under an overall flattening strain. In addition the R_f-ϕ method has yielded the least *k*-value indicating very strong flattening, and this value is attested by sheet-like appearance of many a pebbles.

8. Discussions & Conclusions

8.1. Mode of emplacement: Both of the rocks groups show no field evidence of emplacement in a liquid state, such as chilled margins, feeder dykes or hosting xenoliths of country rocks. This interesting feature of these rocks points towards their emplacement history. Both the KLG and BW rocks are found within polydeformed metasediemnatry rocks

comprising the NSMB assemblage and not within stable cratonic lithologies, which proffers another clue in this regard. Recent workers (Prabhakar *et al*., 2014) have categorized the study area as a tectonic melange and invoked the involvement of the adjacent shear zone (Bangripoosi Shear Zone) in its assembly. Thus, it can be stated that these mafic-ultramafic rocks cannot be characterized as intrusive rocks, but as thrusted tectonic slivers, emplaced within the country rocks during episodes of deformation.

8.2. Structure of the Country Rocks: The metasedimnetary country rock belonging to the Chaibasa Formation of Singhbhum Group have evidences of three phases of deformation- with F1 AP parallel to F2 AP, and F3 AP at a high angle. Evidence indicates co-axial refolding of F1 by F2 and a final phase of ESE-WNW regional compression. Strain analysis of these rocks indicates deformation under an overall flattening strain. The final phase of deformation is marked by an extensive north-south shearing.

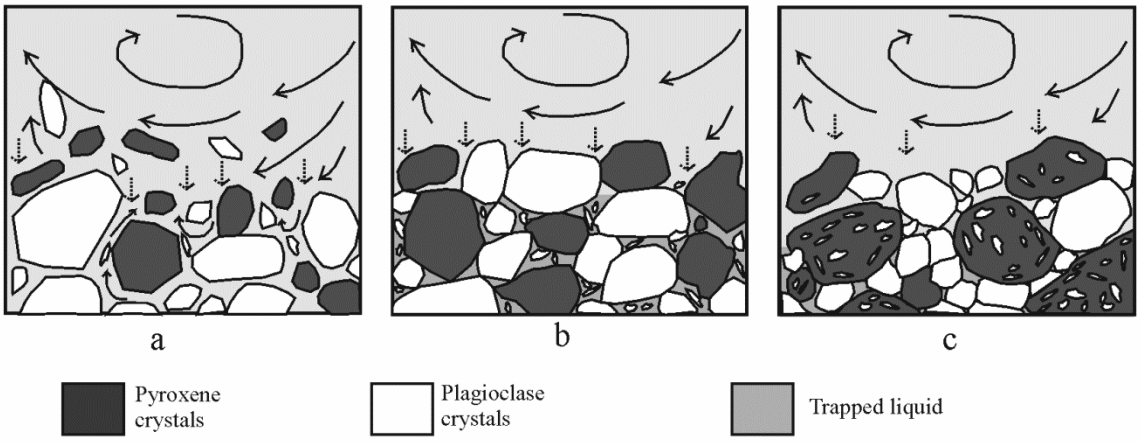

Figure 17: Simplified schematic diagram depicting the interplay between adcumulus growth and textural coarsening process, in the crystallization history of KLG rocks- (a) Plagioclase grains have settled down from the main convecting body of the magma, along with relatively less amounts of pyroxene. The grains grow via adcumulus process and unimpeded circulation of the interstitial liquid with the above magma chamber exists. (b) As a result of adcumulus growth, the grains impinge, cutting off circulation with the convecting chamber and trapping the interstitial liquid. (c) Textural coarsening process commences, arresting further nucleation and enhancing the growth rate. Pyroxenes outgrow the newly formed plagioclase grains, enclosing them to form the observed oikocryst-chadacryst assemblage (Chakraborti *et al*., 2017a).

8.3. Crystallization history of KLG: The layered gabbroic rocks display modal, textural and cryptic layering along with other petrographically diverse features. The presence of poikilitic texture and bi-modal plagioclase grains in some of the layers couldn't be explained by Polybaric Crystallization process, as both modes of plagioclase grains had uniform anorthite content (Chakraborti et al., 2017a). Crystal Size Distribution (CSD) analysis was hence performed on the bi-modally distributed plagioclase grains from the layers with poikilitic texture. The CSD results showed that Textural Coarsening process was responsible

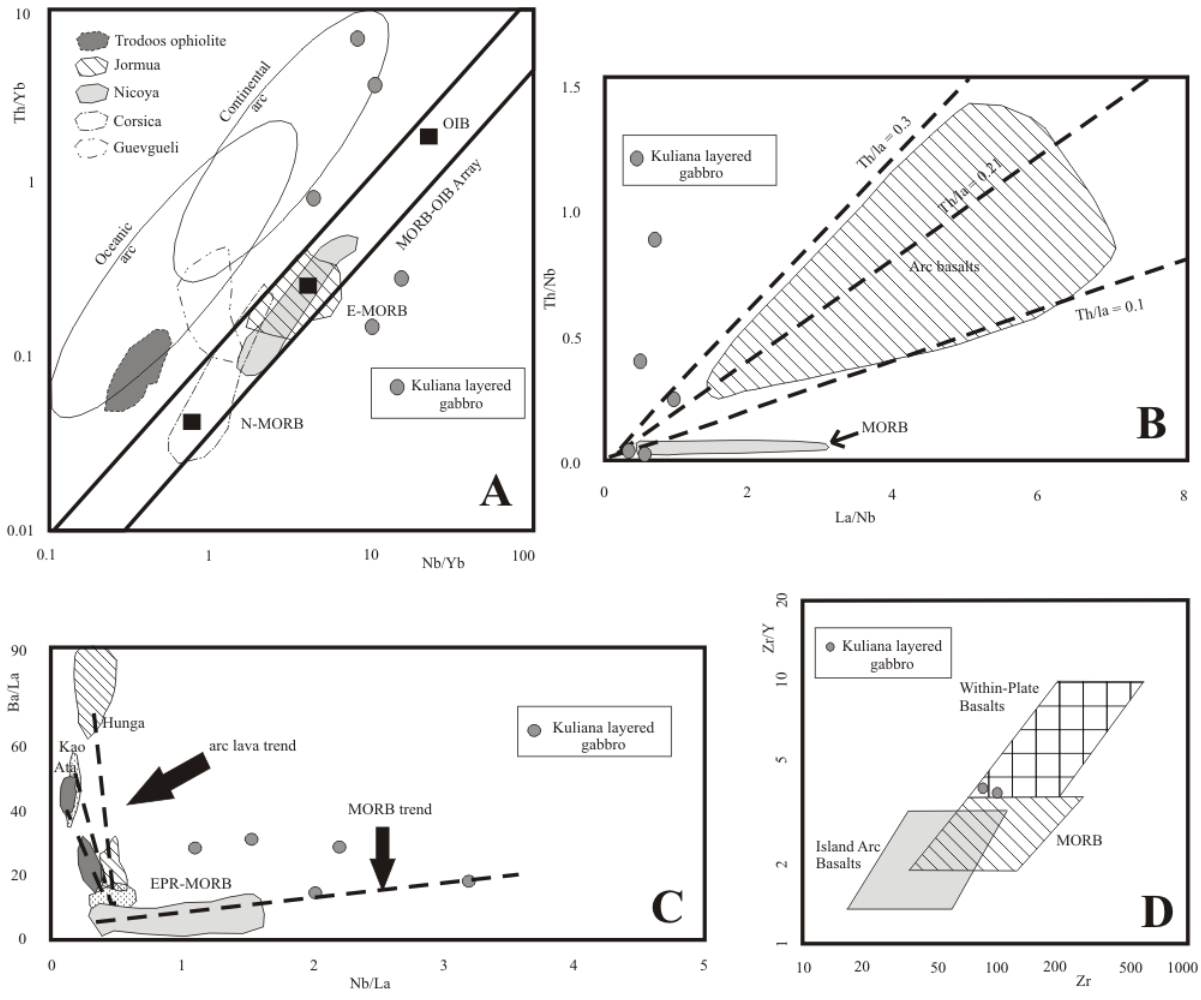

Figure 18: Immobile trace element diagrams showing plots of the calculated parent melts of KLG rocks (Chakraborti *et al.*, 2016). Data taken from Escrig *et al.* (2009); Gao *et al.* (2008); Pearce and Norry, (1979); Pearce (2014).

and a transitional relationship was hypothesized between adcumulus growth and textural coarsening process (Fig. 17)-

1> A progressive increase in crystallinity causes the released latent heat, which was once redistributed by the inter-cumulus melt flow, to get trapped within the cumulus pile.

2> The ambient temperature rises until it reaches the liquidus temperature of the cumulus minerals.

3> Textural Coarsening process takes effect at this point, whereby grains smaller than a critical dimension is resorbed and facilitates the growth of larger grains.

4> This process stops with the lowering of the temperature, and adcumulus process takes over again.

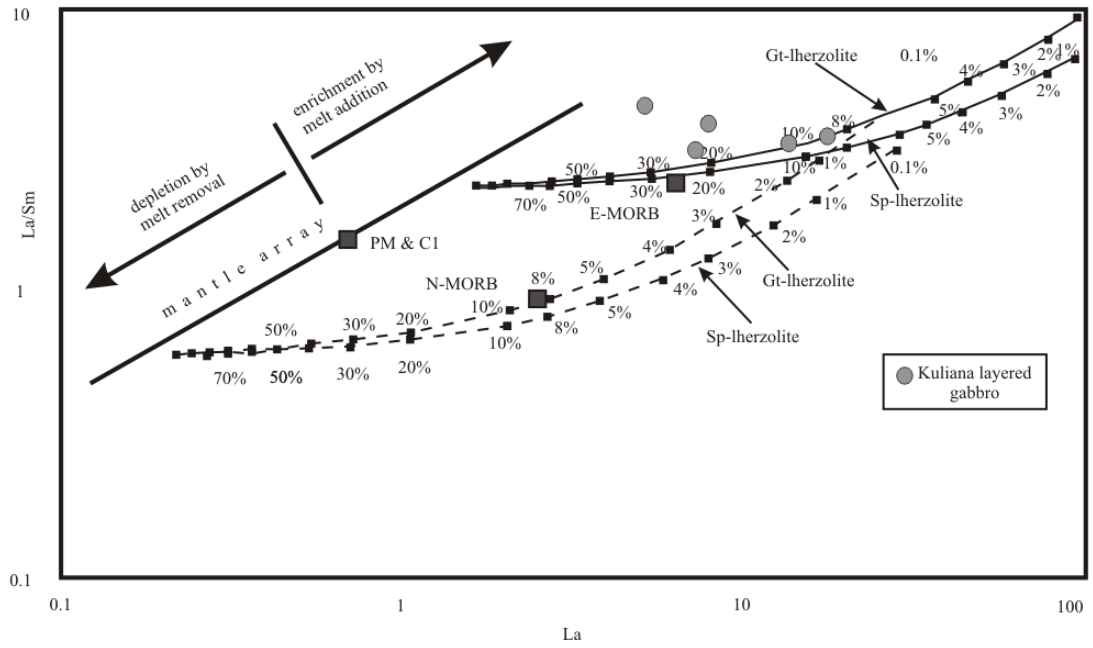

Figure 19: La vs La/Sm diagram (modified after Almandaz 2002) showing melt curves (or lines) obtained using the non-modal batch melting equations of Shaw (1970). Dashed and solid curves (or lines) are the melting trends. Kuliana layered gabbro rocks plot close to E-MORB composition, near the upper melting curve in the Gt-lherzolite facies between regions defined by 8-30% partial melting. [PM: Primitive Mantle; Gt-lherzolite: Garnet lherzolite; Sp-lherzolite: Spinel-Lherzolite.

8.4. Parental melts of KLG: As the cumulate layers of the KLG do not provide information about the parent magma of this, the Equilibrium Distribution Method (EDM) of Bédard (1994) was utilized to estimate trace element concentrations of melts in equilibrium with the cumulate solid products. The calculated parent melts exhibit LREE and LILE enriched nature, marked depletion of Ti and Y and successive total REE depletion through

progressive differentiation. Plotting them in several immobile trace element diagrams (Fig. 18) - Nb/Yb vs Th/Yb, La/Nb vs Th/Nb, Nb/La vs Ba/La and Zr vs Zr/Y, revealed their chemical affinity to enriched MORB like magmas. La vs La/Sm plot of mantle sources (Fig. 19) affected by partial melting show a relatively low degree (8-30%) of melting a deeper (garnet facies) mantle to be the possible source region of the parent magmas of the Kuliana layered mafic suite.

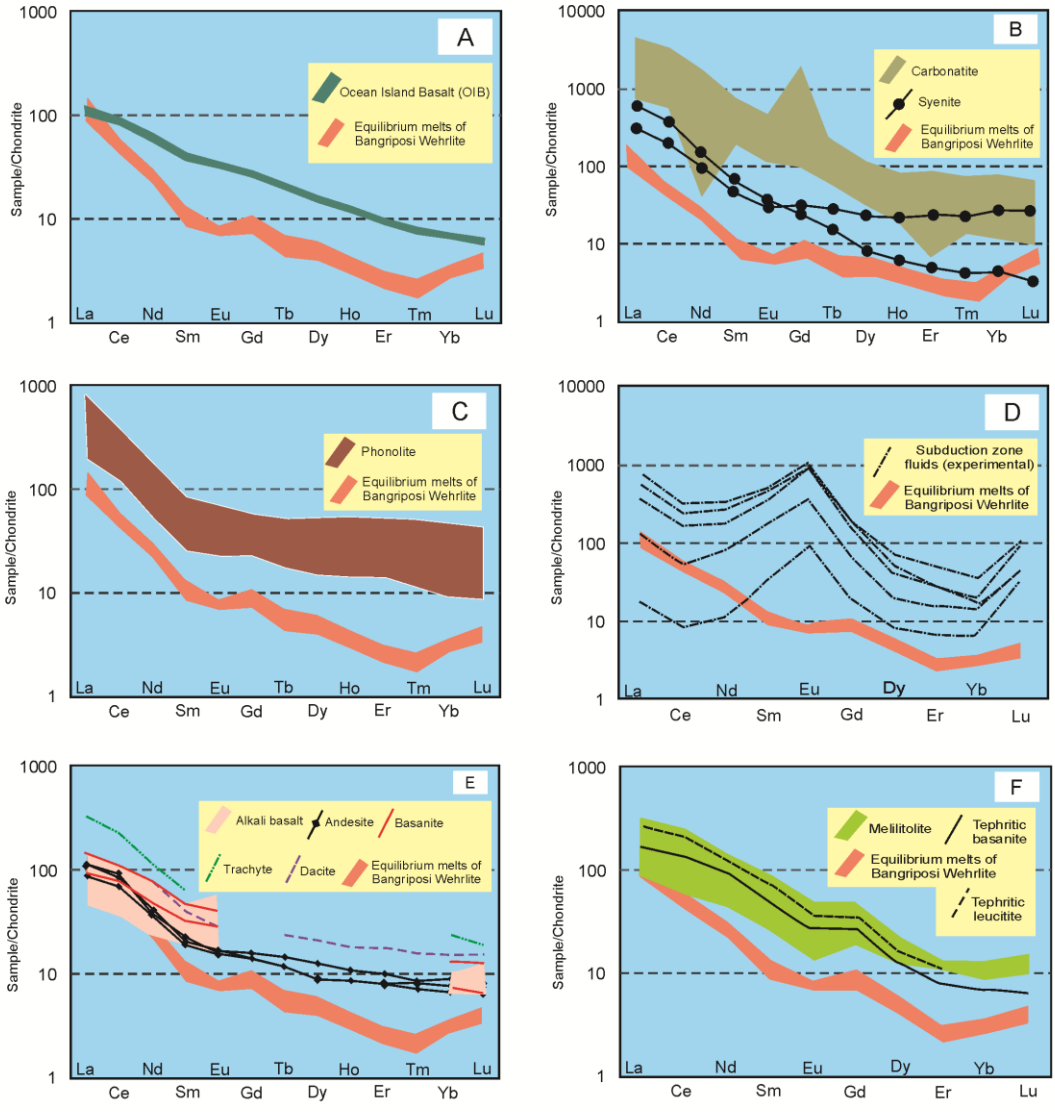

Figure 20: Comparison of chondrite normalized (normalizing values taken from Boynton, 1984) REE distribution patterns of liquids in equilibrium with pyroxene separates from Bangriposi wehrlite rocks with natural melts. The REE patterns of the liquids in equilibrium with pyroxene separates most closely resemble the patterns of phonolites, ultrapotassic rocks and carbonatites to some extent. (Data taken from Aldanmaz et al., 2006; Basu et al., 1991; Cheng et al., 2003; Di Battistini et al., 2001; Hay et al., 1995; Kelly et al., 2008; Kessel et al., 2005; Price et al., 1985; Stoppa and Sharygin, 2009; Taylor and Hallberg, 1977; Ying et al., 2004).

8.5. Metasomatic history of BW: Detailed mineralogical and geochemical studies of the BW rocks have revealed that these rocks have suffered a two-stage alteration involving a deeper level modal and cryptic metasomatism and a subsequent shallower depth pervasive hydrothermal alteration. The deeper level process includes- cryptic metasomatism defined by elevated LREE contents of the wehrlite and its clinopyroxne grains, and modal metasomatism by the absence of primary orthopyroxene grains, presence of secondary diopside- phlogopite (now present as vermiculite) defining disequilibrium reaction textures, and secondary orthopyroxene rims around serpentinized olivine. The mineralogical and geochemical changes due to the metasomatic event present a contrasting picture concerning the metasomatic history of the rocks. Although it is not clear whether the deeper level metasomatism episodes is comprised of a single or multiple melts, an attempt was made to estimate the REE concentrations of the final equilibrating melt from REE contents of clinopyroxene grains of the wehrlite. The possibility of the LREE-enriched equilibrating melt of the wehrlite rocks (the deeper level metasomatic agent) being similar to residual melts from the E-MORB type parental melts of the KLG suite has been ruled out by geochemical modelling (Chakraborti et al., 2017b). REE abundance patterns of several natural enriched melts have been compared with REE pattern of calculated equilibrating, and most resemblance has been observed with calcic and potassic melts (Fig. 20). It is therefore suggested that the Cr-spinel bearing wehrlite rocks of Bangriposi has been affected by a calcio-potassic melt in deeper level, prior to the shallow level serpentinization event.

8.6. Enriched mantle sources: The Sr-Nd isotopic data of the mafic-ultramafic rocks suggest an overall enriched nature of the mantle source present beneath the Singhbhum Craton (SC) in the Mesoarchean period. Nd isotopic compositions of KLG and BW rocks were compared with other Archaean crustal rocks (Fig. 21). KLG rocks show resemblance

towards Isua and OMG supracrustal rocks and with the Bangur Gabbro (Augé et al., 2003) rocks, situated south of the study area. It is also evident from the comparison diagram that the source region of these rocks was slightly more enriched than the crustal rocks. This inference is in accordance with the calculated parent mallets of KLG, which are products of melting of

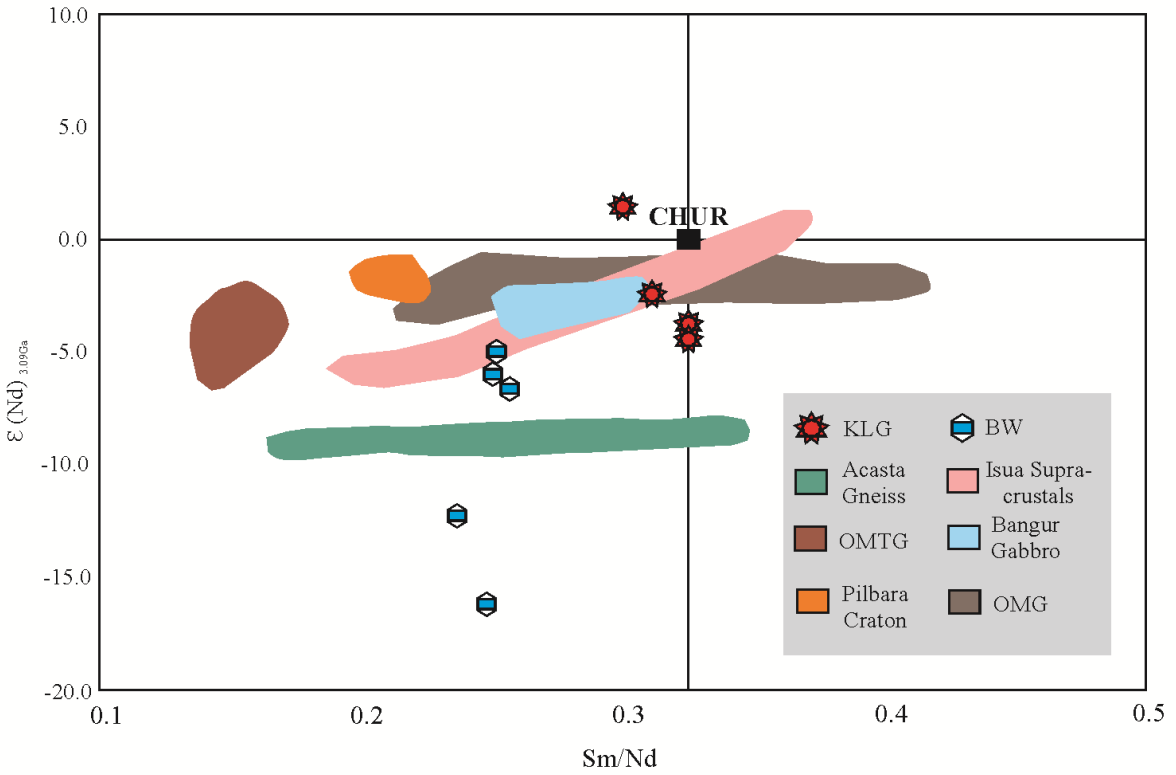

Figure 21: Ɛ (Nd) vs Sm/Nd (3.09 Ga) diagram of BW and KLG rocks, compared with other Archaean crustal rocks. (Data taken from Augé et al., 2003; Moorbath et al., 1997; Sharma et al., 1994; Smithies et al., 2004).

a enriched source, and the composition of the final metsomatic agent of the deeper level metasomatism episode affecting the BW rocks. The estimated composition of the infiltrating melt requires production from a modified and enriched mantle reservoir. Presence of such an enriched mantle reservoir beneath Archaean cratons have been hypothesized by many workers (Cousens et al., 2002; Smithies et al., 2004; Tatsumi, 2000), and generally the reason for enrichment has been attributed to the growing consensus on subduction processes operating in the Archaean era.

9. Summary

Overall, the major findings from the study suggest that these mafic-ultramafic rocks constitute a tectonic mélange, where rocks of different ages have been juxtaposed against each other. The mafic-ultramafic rocks represent tectonic slivers of an ancient oceanic crust, dismembered during thrusting and emplaced in different regions of the Mesoarchean country rocks of Singhbhum Group. Thus, these rocks can be characterized as ophiolitic rocks, vestiges of Archaean subduction processes.

REFERENCES CITED

Aldanmaz, E., Köprübaşi, N., Gürer, Ö.F., Kaymakçi, N., Gourgaud, A., 2006. Geochemical constraints on the Cenozoic, OIB-type alkaline volcanic rocks of NW Turkey: Implications for mantle sources and melting processes. Lithos 86, 50–76. doi:10.1016/j.lithos.2005.04.003

Augé, T., Cocherie, A., Genna, A., Armstrong, R., Guerrot, C., Mukherjee, M.M., Patra, R.N., 2003. Age of the Baula PGE mineralization (Orissa, India) and its implications concerning the Singhbhum Archaean nucleus. Precambrian Res. 121, 85–101. doi:10.1016/S0301-9268(02)00202-4

Banerjee, A., Chakrabarti, R., Mandal, S., 2016. Geochemical anatomy of a spheroidally weathered diabase. Chem. Geol. 440, 124–138. doi:10.1016/j.chemgeo.2016.07.008

Basu, A.R., Wang Junwen, Huang Wankang, Xie Guanghong, Tatsumoto, M., 1991. Major element, REE, and Pb, Nd and Sr isotopic geochemistry of Cenozoic volcanic rocks of eastern China: implications for their origin from suboceanic-type mantle reservoirs. Earth Planet. Sci. Lett. 105, 149–169. doi:10.1016/0012-821X(91)90127-4

Chakraborti, T.M., Ray, A., Deb, G.K., 2017a. Crystal size distribution analysis of plagioclase from gabbro-anorthosite suite of Kuliana, Orissa, eastern India: implications for textural coarsening in a static magma chamber. Geol. J. 52, 234–248. doi:10.1002/gj.2752

Chakraborti. T.M., Ray, A., Deb, G.K., 2017b. Evidence of melt/rock interaction in the Cr-spinel bearing wehrlite rocks of Bangriposi, India: implications for nature of the metasomatic agent. Geosci. Front. Available online on 21st August, 2017. doi: 10.1016/j.gsf.2017.08.001.

Chakraborti, T.M., Ray, A., Deb, G.K., 2016. Computation of Parent Magma Compositions of a Layered Gabbro Suite around Kuliana, Orissa, Eastern India: Implications for Magmatic Evolution and Paleotectonic Setting. J. Geol. 124, 723–741. doi:10.1086/688607

Cheng, X., Zhilong, H., Congqiang, L., Liang, Q., Wenbo, L., Tao, G., 2003. PGE geochemistry of carbonatites in Maoniuping REE deposit, Sichuan Province, China: Preliminary study. Geochem. J. 37, 391–399. doi:10.2343/geochemj.37.391

Cousens, B.L., Aspler, L.B., Chiarenzelli, J.R., Donaldson, J.A., Sandeman, H., Peterson, T.D., LeCheminant, A.N., 2002. Enriched Archean lithospheric mantle beneath western Churchill Province tapped during Paleoproterozoic orogenesis. Geology 29, 827–830. doi:10.1130/0091-7613(2001)029<0827:EALMBW>2.0.CO;2

Di Battistini, G., Montanini, A., Vernia, L., Venturelli, G., Tonarini, S., 2001. Petrology of melilite-bearing rocks from the Montefiascone Volcanic Complex (Roman Magmatic Province): New insights into the ultrapotassic volcanism of Central Italy. Lithos 59, 1–24. doi:10.1016/S0024-4937(01)00054-8

Escrig, S., Bézos, A., Goldstein, S.L., Langmuir, C.H., Michael, P.J., 2009. Mantle source variations beneath the eastern lau spreading center and the nature of subduction components in the lau basin-tonga arc system. Geochemistry, Geophys. Geosystems 10. doi:10.1029/2008GC002281

Gao, Y., Wei, R., Hou, Z., Tian, S., Zhao, R., 2008. Eocene high-MgO volcanism in southern Tibet: New constraints for mantle source characteristics and deep processes. Lithos 105, 63–72. doi:10.1016/j.lithos.2008.02.008

Hay, D.E., Wendlandt, R.F., Wendlandt, E.D., 1995. The origin of Kenya rift plateau-type flood phonolites: Evidence from geochemical studies for fusion of lower crust modified by alkali basaltic magmatism. J. Geophys. Res. 100, 411–422. doi:10.1029/94JB02159

Kelly, P.J., Kyle, P.R., Dunbar, N.W., Sims, K.W.W., 2008. Geochemistry and mineralogy of the phonolite lava

lake, Erebus volcano, Antarctica: 1972–2004 and comparison with older lavas. J. Volcanol. Geotherm. Res. 177, 589–605. doi:10.1016/j.jvolgeores.2007.11.025

Kessel, R., Schmidt, M.W., Ulmer, P., Pettke, T., 2005. Trace element signature of subduction-zone fluids, melts and supercritical liquids at 120–180 km depth. Nature 437, 724–727. doi:10.1038/nature03971

Khanna P.P.; Saini N.K.; Mukherjee P.K.; Purohit K.K. 2009. An appraisal of ICP-MS technique for determination of REEs: long term QC assessment of Silicate rock analysis. Himalayan Geology 30:95–99.

Moorbath, S., Whitehouse, M.J., Kamber, B.S., 1997. Extreme Nd-isotope heterogeneity in the early Archaean — fact or fiction? Case histories from northern Canada and West Greenland. Chem. Geol. 135, 213–231. doi:10.1016/S0009-2541(96)00117-9

Pearce, J.A., 2014. Immobile element fingerprinting of ophiolites. Elements 10, 101–108. doi:10.2113/gselements.10.2.101

Prabhakar, N., Bhattacharya, A., Sathyanarayanan, M., Mukherjee, P.K., 2014. Structural, petrological, and chronological constraints from eastern India and implications for the ~1.0 Ga assembly of greater India. J. Geol. 122, 411–432. doi:10.1086/676459

Price, R.C., Johnson, R.W., Gray, C.M., Frey, F.A., 1985. Geochemistry of phonolites and trachytes from the summit region of Mt. Kenya. Contrib. to Mineral. Petrol. 89, 394–409. doi:10.1007/BF00381560

Saha, A.K. 1994. Crustal evolution of Singhbhum- North Orissa, Eastern India. Geological Society of India.

Sharma, M., Basu, A.R., Ray, S.L., 1994. Sm-Nd Isotopic and Geochemical Study of the Archean Tonalite-Amphibolite association from the eastern Indian Craton. Contrib. to Mineral. Petrol. 117, 45–55. doi:10.1007/BF00307728

Smithies, R.H., Champion, D.C., Sun, S.S., 2004. Evidence for early LREE-enriched mantle source regions: Diverse magmas from the c. 3.0 Ga Mallina Basin, Pilbara Craton, NW Australia. J. Petrol. 45, 1515–1537. doi:10.1093/petrology/egh014

Stoppa, F., Sharygin, V. V., 2009. Melilitolite intrusion and pelite digestion by high temperature kamafugitic magma at Colle Fabbri, Spoleto, Italy. Lithos 112, 306–320. doi:10.1016/j.lithos.2009.03.001

Tatsumi, Y., 2000. Continental crust formation by crustal delamination in subduction zones and complementary accumulation of the enriched mantle i component in the mantle. Geochemistry, Geophys. Geosystems 1. doi:10.1029/2000GC000094

Taylor, S.R., Hallberg, J.A., 1977. Rare-earth elements in the Marda calc-alkaline suite: an Archaean geochemical analogue of Andean-type volcanism. Geochim. Cosmochim. Acta 41, 1125–1129. doi:10.1016/0016-7037(77)90107-7

Ying, J., Zhou, X., Zhang, H., 2004. Geochemical and isotopic investigation of the Laiwu-Zibo carbonatites from western Shandong Province, China, and implications for their petrogenesis and enriched mantle source. Lithos 75, 413–426. doi:10.1016/j.lithos.2004.04.037